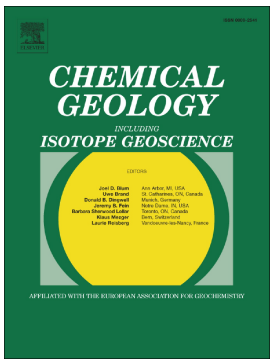

Re-assessment of the effect of fractional crystallization on Mo isotopes: Constraints from I-type granitoids and their enclosed mafic magmatic enclaves

Shuo Chen, Yaoling Niu, Hongmei Gong, Xiaohong Wang, Qiqi Xue

PII: S0009-2541(22)00108-5

DOI: https://doi.org/10.1016/j.chemgeo.2022.120814

Reference: CHEMGE 120814

To appear in: *Chemical Geology*

Received date: 26 April 2021

Revised date: 20 February 2022

Accepted date: 10 March 2022

Please cite this article as: S. Chen, Y. Niu, H. Gong, et al., Re-assessment of the effect of fractional crystallization on Mo isotopes: Constraints from I-type granitoids and their enclosed mafic magmatic enclaves, *Chemical Geology* (2021), https://doi.org/10.1016/j.chemgeo.2022.120814

Re-assessment of the effect of fractional crystallization on Mo isotopes: constraints from I-type granitoids and their enclosed mafic magmatic enclaves

Shuo Chen[1,2,3]*, Yaoling Niu[2,4,5], Hongmei Gong[1,2,3], Xiaohong Wang[1,2,3], Qiqi Xue[1]

[1]Institute of Oceanology, Chinese Academy of Sciences, Qingdao 266071, China

[2]Laboratory for Marine Geology, Qingdao National Laboratory for Marine Science and Technology, Qingdao 266061, China

[3]Center for Ocean Mega-Science, Chinese Academy of Sciences, 7 Nanhai Road, Qingdao, 266071, China

[4]Department of Earth Sciences, Durham University, Durham DH1 3LE, UK

[5]China University of Geosciences, Beijing 100083, China

Corresponding author: Shuo Chen (shuochen@qdio.ac.cn)

Full postal address: Institute of Oceanology

Chinese Academy of Sciences

Qingdao

266071

China.

Abstract

In recent years, considerable progress has been made on the study of Mo isotopes in high-temperature geological processes. However, it is still controversial whether Mo isotope fractionation occurs during magmatic differentiation. Here we reassess the effect of magma differentiation on Mo isotope fractionation using published data in conjunction with our new analysis of Mo isotopes in well-characterized I-type granitoids and their enclosed mafic magmatic enclaves (MMEs) from two plutons in the North Qilian Orogen. The MMEs in each pluton, representing earlier cumulates with greater modal proportions of amphibole and biotite, show similar Mo elemental and isotopic compositions to their host granitoids. The absence of covariation of Mo isotopes with Dy/Dy*, Fe_2O_3 and K/Rb in both plutons further indicates that fractional crystallization of amphibole, biotite and Fe^{3+}-rich minerals does not fractionate Mo isotopes in these granitoids. On the basis of re-assessment of published and our newly obtained Mo isotope data, we find that there is no clear evidence for Mo isotope fractionation during fractional crystallization in igneous rock. Instead, Mo isotopes of our samples correlate positively with Sr isotopes and Rb/La ratios, and negatively with Nd isotopes and Ce/Pb ratios, indicating clearly that magma source compositional variation controls the variation of Mo isotope compositions of these granitoids.

Keywords: Mo isotopes, Granitoids, Fractional crystallization, Source heterogeneity, Continental crust

1 Introduction

Molybdenum is a redox-sensitive element that has seven stable isotopes. Surface cycling of elemental Mo can lead to large isotopic fractionations, notably with preferential sorption of its light isotopes onto ferro-manganese coatings, resulting in seawater with an isotopically heavy composition (Barling et al., 2001). Under reducing conditions, however, Mo is near-quantitatively removed from seawater, resulting in little or no isotope fractionation between the euxinic sediments and the ocean (e.g., Barling et al., 2001, 2004). These behaviors have enabled Mo isotopic data to be used for reconstructing ocean paleo-redox conditions (Arnold et al., 2004; Goldberg et al., 2009; Pearce et al., 2008; Siebert et al., 2003), and for tracing surface materials that may have been subducted and transported to mantle source regions of basaltic arc magmas (Freymuth et al., 2015, 2016; König et al., 2016; Zhang et al., 2020).

Although equilibrium mass-dependent isotope fractionation is suggested to be smaller at high temperatures, recent studies on high-temperature materials, such as komatiites (Greber et al., 2015; McCoy-West et al., 2019), oceanic basalts (Liang et al., 2017; Bezard et al., 2016), Icelandic lavas (Yang et al., 2015), arc lavas (Voegelin et al., 2014; Freymuth et al., 2015, 2016; König et al., 2016; Willbold et al., 2018; Villalobos-Orchard et al., 2020), molybdenite deposits (Breillat et al., 2016), and granites (Yang et al., 2015; Fan et al., 2020) have shown that $\delta^{98/95}$Mo (relative to NIST SRM 3134 standard) variation in magmatic systems exceeds 2‰. The $\delta^{98/95}$Mo of arc lavas show considerable variation, with a span greater than 1.5‰ and a weighted mean of 0.07 ± 0.68‰ (N = 133, 2SD; Villalobos-Orchard et al., 2020), significantly higher than that of the depleted mantle (-0.21 ± 0.02‰; Willbold and Elliott, 2017). It has been suggested that the isotopically heavy Mo in arc lavas may reflect addition of slab-derived components to their mantle source (Freymuth et al., 2015, 2016; Ko¨nig et al., 2016; Gaschnig et al., 2017;

Villalobos-Orchard et al., 2020). However, some authors have argued that the high $\delta^{98/95}$Mo values in some arc lavas are caused by fractional crystallization of hydrous phases such as hornblende and biotite preferentially incorporating light Mo isotopes (Voegelin et al., 2014; Wille et al., 2018). This likely adds to the complexity of the Mo isotope systematics inherent to subduction zones. If the effect of fractional crystallization on Mo isotopes is significant, it means that Mo isotopes of evolved samples cannot be directly used for tracing their sources unless the effect is quantified and can be corrected. However, this is currently controversial as no Mo isotope fractionation was observed during magma differentiation for a suite of basalts to rhyolites from Hekla volcano (Yang et al., 2015), hydrous lavas from Mariana, Izu and arc lavas from Lesser Antilles Arc (Freymuth et al., 2015, 2016; Gaschnig et al., 2017; Villalobos-Orchard et al., 2020) and mid-ocean ridge basalts (MORB) (Bezard et al., 2016; Chen et al., 2022). These contrasting results are yet to be reconciled because most of these sample sets do not represent a cogenetic suite

Granitoids, especially I-type granites, have great potential for deciphering the possible effect of fractional crystallization on Mo isotopes because they contain hydrous minerals (e.g., amphibole and biotite), and because fractional crystallization has been widely regarded as a significant cause for compositional variations of granitoids (Lee and Bachmann, 2014; Lee and Morton, 2015). However, recent studies on Mo isotopes in granitic rocks also show different results. Yang et al. (2017) observed that $\delta^{98/95}$Mo was negatively correlated with Fe_2O_3 contents and K/Rb ratios for I-type granites from the Lachlan Fold Belt in Australia and the Loch Doon, Criffell and Fleet pluton in Scotland and suggested that light Mo isotopes are preferentially incorporated in hornblende and Fe^{3+}-rich minerals during granitic magma differentiation. In contrast, Fan et al. (2020) showed the absence of correlations between $\delta^{98/95}$Mo values and

magma differentiation indicators in granodioritic porphyries and granodiorite from central-eastern China and concluded that fractional crystallization cannot account for Mo isotopes variation in these granitic rocks.

In order to reconcile the above debate and genuinely understand the behavior of Mo isotope during fractional crystallization, we have analyzed Mo isotopes for two cogenetic suites of well-characterized I-type granitoids and their enclosed mafic magmatic enclaves (MMEs) from the North Qilian Orogenic Belt (Chen et al., 2015; 2016). We then re-assess published Mo isotopes (Freymuth et al., 2015, 2016; Gaschnig et al., 2017; Voegelin et al., 2014; Villalobos-Orchard et al., 2020; Yang et al., 2015) for magmatic data sets in the light of our results and find no clear evidence for Mo isotope fractionation during fractional crystallization in igneous rock. Instead, our data suggest that compositional variation in magma source regions exerts significant control on the observed Mo isotope variation of igneous rocks.

2 Geological background and samples

The vast Greater Tibetan Plateau has been amalgamated through sequential accretion of several microcontinents, island arcs, and flysch complexes onto the southern margin of Eurasia since the early Paleozoic (Yin and Harrison, 2000). This accretion involved several continental collision events with suture zones characterized by syn-collisional granitoid batholiths that young progressively towards the south. The syn-collisional granitoid batholith associated with the North Qilian suture (NQS) is located in the North Qilian Orogenic Belt (NQOB), which extends NW-SE for more than 1000 km (Fig. 1). The NQOB consists of two ophiolite belts, volcanic and granitic rocks, high pressure (HP) metamorphic rocks, and accretionary complexes (see review by Song et al., 2013). The southern ophiolite belt (ca. 550-497 Ma) mainly comprises pillow basalts, peridotite and ultramafic cumulate of ocean ridge origin (Hou et al.,

2006). The northern ophiolite belt (ca. 490-448 Ma) consists of ultramafic rocks, MORB, cumulates, supra-subduction zone (SSZ) basalts, and pelagic-hemipelagic siliceous-argillaceous rocks, which has been suggested to have formed in a back-arc setting (Xia et al., 2003; Xia and Song, 2010). The Cambrian-Ordovician arc complex (ca. 516-446 Ma) located between the two ophiolite belts consists of felsic calc-alkaline volcanic rocks, boninitic complexes and granitoid plutons (Xia et al., 2012). Previous studies suggested that the Central Qilian block collided with the Alxa block in the Early Silurian (Fig. 1; see Song et al., 2013), producing voluminous syn-collisional magmatic rocks between ca. 440 and 420 Ma (Chen et al., 2016, 2018; Song et al., 2013; Tseng et al., 2009; Yu et al., 2015). The Qumushan (QMS) and Baojishan (BJS) granitoid plutons (ca. 430 Ma) we studied are in the eastern segment of the NQOB (Fig. 1b).

The QMS and BJS granitoids are of diorite to granodioritic composition and contain ubiquitous MMEs with varying size and shape (Chen et al., 2015, 2016). In this study, we selected several fresh bulk rocks of host-MME sample pairs from the two plutons for studying Mo isotopes. Previous studies showed that the MMEs are diorite in composition, which consists of amphibole (~30–50 vol%), plagioclase (~40–50 vol%), biotite (~2–20 vol%), quartz (~ 10 vol%), alkali feldspar (<10 vol%) and accessory phases such as zircon, apatite, magnetite, and titanite (Chen et al., 2015, 2016). These MMEs generally have finer grain size than their host granodiorites and they show neither textures of crystal reactive overgrowth nor chilled margins (Chen et al., 2015, 2016). A more detailed study of mineral mapping using a TESCAN Integrated Mineral Analyzer (TIMA) system has confirmed that the MMEs generally have the same mineralogy as their host granodiorites except that they have greater abundances of mafic phases (e.g. amphibole and biotite) (Chen et al., 2021; Fig. A1). The bulk-rock major, trace elements, Sr-Nd isotopes, and zircon U-Pb age and in-situ O isotopes are previously reported

(Chen et al., 2015, 2016, 2021) and compiled in Table A1. Compositionally, the host granodiorites and their enclosed MMEs are calc-alkaline and weakly peraluminous to metaluminous, which is typical of I-type granitoids (Fig. A2; Chappell and White, 1992).

The petrogenesis of MMEs has been a controversial topic and a variety of models have been proposed (Barbarin, 2005), including (i) refractory and residual phase assemblages (Chappell and White, 1991; Chappell et al., 1987), (ii) foreign xenoliths (e.g., Vernon, 1983; Xu et al., 2006), (iii) magma mixing of mantle-derived basaltic melt and crust-derived felsic melt (e.g., Barbarin, 2005; Barbarin and Didier, 1991; Chen et al., 2013a), (iv) early-formed cumulate of co-genetic crystals (e.g., Chen et al., 2015, 2016; Dahlquist, 2002; Dodge and Kistler, 1990; Donaire et al., 2005; Niu et al., 2013). Previous studies have suggested that the MMEs in QMS and BJS plutons in this study are best understood as early-formed 'cumulate' of the same magmatic system as their host granitoids. This is based on several lines of evidence: (i) the MMEs in our study have the same mineral assemblage (Fig. A1) and similar mineral compositions to those of their host granitoids; (ii) amphibole and plagioclase crystals with uniform composition show absence of disequilibrium textures in both the MMEs and their host granitoids; (iii) their different mineral modal proportions are responsible for the compositional difference between them and their host granitoids; (iv) more importantly, the bulk-rock radiogenic isotopes (e.g., Sr-Nd isotope) and in-situ zircon O isotopes of the MMEs are indistinguishable from those of their host granitoids (Fig. A3) (Chen et al., 2015, 2016, 2021; Xiao et al., 2020).

3 Analytical methods

Fresh rock samples were crushed to small pieces, and handpicked to avoid fractures and veins, which were then washed in distilled Milli-Q water several times using an ultrasonic bath

and powdered to 200 meshes in an agate mortar for bulk-rock Mo isotope analysis. Mo isotope analysis was performed using a multi-collector inductively coupled plasma mass-spectrometer (MC-ICPMS; Nu plasma II) in low-resolution mode at the Laboratory of Ocean Lithosphere and Mantle Dynamics, Institute of Oceanology, Chinese Academy of Sciences (IOCAS). Chemical protocols and data reduction are largely based on those presented in Willbold et al. (2016) and Chen et al. (2022). A brief description is given below.

Variable amounts of sample powders were weighed into 15 ml PTFE vial according to their Mo concentration. For every 50 mg of sample, 1mL reverse aqua regia (HNO_3: HCl = 3:1) and 0.5 mL HF was added in the vial, which was then inserted and sealed in a high-pressure metal bomb, and heated in an oven at 190 °C for 15-48 hours. The sample solution was then transferred to a 60mL Savillex PFA vial and evaporated to incipient dryness and re-dissolved in 6M HCl until it was completely dissolved. Appropriate mixed ^{97}Mo–^{100}Mo tracer of known composition was added to each sample to correct for possible mass-dependent isotope fractionation occurring during chemistry and mass-spectrometry. Molybdenum was separated from the sample matrix by a single pass anion exchange column, using an Eichrom 200-400 mesh 1×8 anion exchange resin following Willbold et al. (2016). Sample solutions containing ~50-70 ng/g Mo were introduced with an Aridus III desolvating PFA nebulizer and analyzed by MC-ICP-MS. We monitored ^{99}Ru as well as ^{101}Ru in the course of analysis to correct for isobaric interferences of ruthenium (Ru) on masses 98 and 100 with the following cup configuration: ^{94}Mo-^{94}Zr-L4, ^{95}Mo-L3, ^{96}Mo-L2,^{97}Mo-L1, ^{98}Mo-^{98}Ru-AX, ^{99}Ru–H1, ^{100}Mo-^{100}Ru-H2, ^{101}Ru–H3. A previous study has observed in double spiked isotope analyses, average compositions of the reference standard within a measurement session often deviate slightly from zero (e.g., Hin et al., 2013). This drift was corrected by subtracting the average composition of NIST SRM 3134 in

a measurement session from each sample analysis in the same session. All Mo isotope measurements herein are reported relative to NIST standard reference material SRM 3134 where $\delta^{98/95}$Mo = 0‰ as convention dictates: $\delta^{98/95}$ Mo=[(^{98}Mo/^{95}Mosample/^{98}Mo/^{95}Mo$_{\text{NIST SRM3134}}$)-1]. The external reproducibility of Mo isotope data was determined from repeated measurements of our in-house standard GSB Mo solution (an ultrapure single elemental standard solution from the China Iron and Steel Research Institute), which yielded an average of $\delta^{98/95}$ Mo=-0.220±0.046 (2SD, n=46). Replicated digestions and measurements of geological reference materials (GRM) (W-2a, BHVO-2, GSP-2, AGV-2, see Table A2), which were analyzed with our samples during the measurements sessions, are in agreement with previously published values within error (Bezard et al., 2016; Burkhardt et al., 2014; Fan et al., 2020; Gaschnig et al., 2017; König et al., 2016; Liang et al., 2017; Yang et al., 2015; Chen et al., 2019; Kaufmann et al., 2021). The total procedural blanks are 0.2ng to 0.48 ng for Mo, which is negligible for the samples.

4 Results

Molybdenum isotopic data of granitoids and the enclosed MME pairs are reported in Table A2. The host granitoids from the BJS pluton show low Mo concentrations ranging from 33 to 77 ng/g and slightly variable $\delta^{98/95}$Mo (0.12±0.04‰ to 0.27±0.05‰), and their enclosed MMEs show slightly higher Mo concentrations (60 to 141 ng/g) but similar $\delta^{98/95}$Mo (0.18 ± 0.03‰ to 0.32±0.05‰), except for sample BJS-08MME with lighter Mo isotopes ($\delta^{98/95}$Mo =-0.08‰±0.06‰). The Mo concentrations of the QMS host granitoids range from 128 to 168 ng/g, which is slightly lower than that of their MMEs (132 to 299 ng/g). However, the $\delta^{98/95}$Mo values of the QMS host granitoids (-0.20±0.01‰ to -0.04±0.04‰) are indistinguishable from their MMEs (-0.26±0.05‰ to -0.03±0.04‰). It is worth noting that although $\delta^{98/95}$Mo values of our samples from the two plutons are distinct, the range of $\delta^{98/95}$Mo values for all host

granitoids and their enclosed MMEs of the same pluton are generally indistinguishable (Fig. 3).

5 Discussion

5.1 Re-assessing the effect of magma differentiation on Mo isotope

It has been well documented, both in natural samples and from theoretical calculations, that stable isotopes of a number of metals (e.g. Fe, Zn, Zr) can be fractionated during magma differentiation (Teng et al., 2008; Inglis et al., 2019; Chen et al., 2013b). Although a number of studies of Mo isotopes have been carried out on igneous rocks with different geological settings in recent years, whether Mo isotope fractionation occurs during fractional crystallization remains controversial.

Voegelin et al. (2014) reported Mo isotopic composition for a suite of hydrous basaltic to rhyolitic samples from a volcano-plutonic suite from Kos Plateau Tuff in the Aegean Arc. The range of $\delta^{98/95}$Mo (0.05 to 0.35‰; normalized to NIST 3134 =0‰) for these samples is suggested to be caused by fractional crystallization. They showed that Mo concentration increased with indicators of fractional crystallization (SiO_2) from basalt to dacite, but abruptly decreased from dacite to rhyolite (Fig. 4a). In contrast, they observed a positive correlation of $\delta^{98/95}$Mo and SiO_2 contents from basalt to rhyolite in these samples (Fig. 4b). Voegelin et al. (2014) further showed that $\delta^{98/95}$Mo of the hornblende and biotite mineral separates were ~ 0.5‰ lower than that of their host dacitic melts. They thus conclude that fractional crystallization of these hydrous phases with isotopically light Mo could account for the observed trend. However, these observations are in sharp contrast with recent studies of a group of volcanic rocks from Hekla volcano in Iceland. These also range in composition from basalt to rhyolite (Yang et al., 2015), but unlike the sample sets from Kos island, samples from Hekla exhibit: (1) a continuous

increase of Mo concentrations with SiO_2 from basalt to rhyolite, indicating that Mo behaves highly incompatibly during fractional crystallization (Fig. 4a) and (2) uniform Mo isotopic compositions ($\delta^{98/95}$Mo= -0.15 ± 0.05‰) with no correlations between $\delta^{98/95}$Mo and SiO2 or Mo content (Fig. 4b) (Yang et al., 2015). A petrographic study of the Hekla samples showed that the major crystallizing phases are anhydrous (olivine, clinopyroxene and plagioclase), along with accessory apatite, magnetite and minor zircon (Savage et al., 2011). Yang et al. (2015) thus suggested that in contrast to hydrous phases, crystallization of anhydrous phases does not fractionate Mo isotopes. Although this seems to reconcile the above-mentioned difference between Kos Island and Hekla, it needs further scrutiny (see below).

In general, arc magmas are enriched in H_2O (Plank et al. 2013) and can stabilize amphibole at pressures corresponding to the middle and lower crust (e.g., Grove et al. 2003; Alonso-Perez et al. 2009). Although amphibole is rarely present as a phenocryst phase in arc lava (Davidson et al. 2007), the relationships between La/Yb, Dy/Yb and SiO_2 contents indicate that removal of amphibole is widespread during differentiation of arc magma, a phenomenon termed "cryptic amphibole fractionation" (Davidson et al. 2007). Recently, Dy/Dy* has also been proved to be an effective indicator of amphibole fractionation during magma evolution, where $Dy/Dy^*=Dy_N/(La_N^{4/13}\times Yb_N^{9/13})$ (Davidson et al., 2013). To test the effect of amphibole fractionation on Mo isotopes, we investigated Dy/Yb, Dy/Dy* and $\delta^{98/95}$Mo variations of different arc lavas, including Kos island, Lesser Antilles Arc, Banda Arc, Mariana Arc and Izu Arc (Freymuth et al., 2016; Freymuth et al., 2015; Gaschnig et al., 2017; Voegelin et al., 2014; Villalobos-Orchard et al., 2020), and compared them to trends for Hekla lavas. As illustrated in Fig. 4, when considering all available arc data, there exists a weak negative trend between

Dy/Yb, Dy/Dy* and SiO_2, but no obvious trend between $\delta^{98/95}$Mo and SiO_2. The co-variation of $\delta^{98/95}$Mo with Dy/Dy* and Dy/Yb is also absent for available arc data (Figs. 5a-b).

As noted by Davidson et al. (2013), it is important to use cogenetic rock suites to identify petrogenetic processes rather than combining samples from different regional suites. Taking each arc system individually, only samples from Kos island and Hekla show clear signs of amphibole fractionation as evidenced by negative trends between Dy/Yb, Dy/Dy* and SiO_2 (Figs. 4c-d). For Hekla lavas, this is seemly at odds with the petrographic observation that the major crystallizing phases were anhydrous (Savage et al., 2011; Yang et al., 2015). However, studies of melt inclusions in iron-rich olivine from Hekla lavas showed that H_2O content in the melts before the eruption was as high as 3.3–6.2 wt% (Portnyagin et al., 2012), indicating that amphibole could have crystallized as a cryptic phase, consistent with our new finding in Figs. 4 c-d. We further explore the relationship between $\delta^{98/95}$Mo with Dy/Yb and Dy/Dy* for samples from Kos island and Hekla. Unsurprisingly, the Hekla lavas show constant $\delta^{98/95}$Mo with decreasing Dy/Yb and Dy/Dy* (Figs. 6a-b), confirming the absence of Mo isotope fractionation during magma differentiation. The variation of $\delta^{98/95}$Mo for the Kos island samples is more complex as the trend towards heavier $\delta^{98/95}$Mo with decreasing Dy/Dy* is determined by a sharp, step increase in $\delta^{98/95}$Mo with the low $\delta^{98/95}$Mo side being defined by only two basaltic samples (Fig. 6a). In addition, the co-variation of $\delta^{98/95}$Mo and Dy/Yb is not observed (Figs. 6b).

To further test the effect of crystal fractionation on Mo isotopes, we made a Rayleigh fractionation model, using the following equation (Allègre, 2008):

$$\delta^{98/95}\mathrm{Mo}_{melt} = (\delta^{98/95}\mathrm{Mo}_{melt0} + 1000) \times \left(f_{Mo}\right)^{(\alpha-1)} - 1000 \qquad (1)$$

Where $\delta^{98/95}Mo_{melt0}$ and $\delta^{98/95}Mo_{melt}$ refer to $\delta^{98/95}Mo$ values of initial melt and residual melt, respectively; α represents Mo isotope fractionation factor between the crystallized mineral and melt; f_{Mo} is the fraction of Mo remaining in the melt, which can be calculated by:

$$f_{Mo}=F\times\frac{C^{Mo}_{melt}}{C^{Mo}_{melt0}} \quad (2)$$

Where F is the fraction of melt remaining; C^{Mo}_{melt} and C^{Mo}_{melt0} refer to Mo concentration in residual melt and initial melt, respectively. The concentration of a given element of the melt can be calculated by:

$$C^{i}_{melt}=C^{i}_{melt0}\times F^{(D^{i}-1)} \quad (3)$$

Where D^{i} refers mineral/melt partition coefficient. A fractionation factor for amphibole ($\alpha_{Amp\text{-}melt}$) of 0.9995 (Voegelin et al., 2014) and variable D^{Mo}_{Amp} (0.1, 0.2 and 0.3) are used in the models (Figs. 6a-b). It can be seen that although the Hekla samples could be reproduced with D^{Mo}_{Amp} of 0.1 to 0.3, this range in D^{Mo}_{Amp} is unable to reproduce the trend for Kos samples (Figs. 6a-b). Moreover, it is notable that amphiboles unlikely represent 100% of the fractionation assemblage as necessary to generate the high α and the D^{Mo}_{Amp} of amphibole determined by Voegelin et al. (2014) was lower than the above modeling (~0.07 to 0.11). This means that the effect of magma differentiation on Mo isotope fractionation should be much smaller than those modelings shown in Figs. 6a-b.

In addition, the potential combined effects of fractional crystallization of biotite and amphibole have also been modeled with varying mineral assemblages (Figs. 6c-d). For simplicity, we use the 'best-estimated' values of D^{Mo} (D^{Mo}_{Amp}=0.10 and D^{Mo}_{Bt}=0.15) and $\alpha_{mineral\text{-}melt}$ (

$\alpha_{Amp\text{-}melt}$ =0.9995 and $\alpha_{Bt\text{-}melt}$ =0.9997) for amphibole and biotite from Vogelin et al. (2014) in these models (Figs. 6c-d). As shown in Figs. 6c-d, although fractional crystallization of an assemblage of 40% amphibole and 60% biotite could roughly reproduce the trend between $\delta^{98/95}$Mo and Dy/Dy* for Kos samples, it fails to reproduce trend between $\delta^{98/95}$Mo and Dy/Yb. More importantly, the above, best-case example requires a large degree of fractional crystallization (>90%), which is in turn at odds with the above assemblage (40% amphibole and 60% biotite) in the modeling as amphibole and/or biotite are not the dominated phases at the late stage of magmatic differentiation. Thus, we suggest that magma differentiation may not be the primary cause for the different behavior of Mo isotope between Hekla and Kos island samples. Furthermore, it is worth noting that Hekla samples not only show uniform $\delta^{98/95}$Mo but also uniform Mo/Ce ratios (Fig. 5c), indicating that Mo and Ce have behaved with similar incompatibility during fractional crystallization. In contrast, the lavas from Kos island, Izu, Mariana and Banda Arc show notable variability in both $\delta^{98/95}$Mo and Mo/Ce ratios (Fig. 5c), suggesting that this variability most likely results from subduction zone processes rather than fractional crystallization. The detailed cause on $\delta^{98/95}$Mo variability for each arc system is beyond the scope of this study, but the above discussion suggests that there is no direct and clear evidence for Mo isotope fractionation during magma differentiation.

5.2 Absence of Mo isotope fractionation during I-type granitoid magma differentiation

It has been suggested that surface weathering of granitoids can significantly fractionate Mo isotopes (Archer and Vance, 2008; Wang et al., 2018). Our samples are fresh with low "chemical index of alteration" (CIA) (<50) (Table A1), suggesting that these samples are not significantly affected by chemical weathering. In addition, their Mo isotope compositional variation (i.e., $\delta^{98/95}$Mo) show no correlation with CIA or LOI (loss on ignition) (Fig.

A4)indicating that the variation of Mo isotopes of our samples is unlikely caused by surface weathering.

It has been proposed that biotite and amphibole are the major hosts for Mo in igneous rocks (Voegelin et al., 2014) as Mo follows similar substitution patterns as Ti. However, Greaney et al. (2018) recently showed that biotite and amphibole contain low Mo contents, which contributes no more than a quarter of bulk-rock Mo in a granitoid. In this study, the MMEs, representing earlier cumulates with greater proportions of amphibole and biotite (Fig. A1), show similar Mo concentration level as their host granitoids in each pluton (Fig. 2a), implying that amphibole and biotite may not be the major hosts for Mo in granitic rocks. The Dy/Dy* ratios of MMEs and their host rocks exhibit a negative correlation with SiO_2 (Fig. 2b), confirming that Dy/Dy* is a robust indicator of amphibole crystallization (Davidson et al., 2013). As illustrated in Fig. 2c, there is no correlation between Mo concentration and Dy/Dy* ratios in the MMEs and host rocks, re-affirming that amphibole is not a major host for Mo. On the other hand, Yang et al. (2017) suggested that elevated K/Rb ratios in granites reflect higher proportion of amphibole because amphibole has been reported to have higher partition coefficient of K over Rb than other crystalline phases. This suggested trend is, however, not observed (Fig. 2d). Thus, K/Rb ratios may not be an applicable indicator for amphibole crystallization in granitoid magmas in our study. In the case of our study, it has been previously suggested that the QMS and BJS MMEs and their host granitoids are cogenetic, with the former representing early-formed cumulates that have greater abundances of mafic phases (amphibole and biotite) (Fig. A1; Chen et al., 2021). They are thus prime sample suites to explore the effect of fractional crystallization on Mo isotopes, especially for crystallization of hydrous phases. As shown in Fig. 3a, while the two plutons display distinct Mo isotopes, the MMEs in each pluton generally show similar Mo

isotopic composition to that of their host granitoids. The lack of clear Mo isotope covariation with indices of magma differentiation (e.g., SiO_2) indicates insignificant Mo isotope fractionation during granitoid magma differentiation. Moreover, the absence of covariation of Mo isotopes with Dy/Dy*, Fe_2O_3 and K/Rb in both plutons (Figs. 3b-d) further indicates that fractional crystallization of minerals such as amphibole, biotite and other Fe^{3+}-rich minerals are unlikely to cause any detectable Mo isotope fractionation. Thus, the new Mo isotope data presented here for cogentic MMEs and their granitoid hosts, combined with our re-assessment of literature data, suggest no clear evidence supporting Mo isotope fractionation during fractional crystallization of igneous rocks. Nevertheless, we do not wish to conclude from our study that Mo isotopes can never be fractionated during fractional crystallization in all cases, as the current database on this issue is still limited. More studies on Mo isotopes of well-characterized, cogenetic samples with well-defined liquid lines of descent from varying settings are needed to further address this controversial issue.

5.3 Source heterogeneity controls Mo isotope variations in granitoids

The lack of co-variation of Sr-Nd isotopes with SiO_2 and MgO of the BJS and QMS MMEs and their host granitoids suggests that crustal assimilation during fractional crystallization is insignificant (Fig. A3; Chen et al., 2015, 2016). Therefore, the differences in Sr and Nd isotopic compositions between the BJS and QMS plutons are most likely inherited from their magma source. The broad positive correlation between $\delta^{98/95}$Mo and $^{87}Sr/^{86}Sr_{(i)}$ and negative correlation between $\delta^{98/95}$Mo and $\varepsilon Nd_{(t)}$ in the two plutons from our study as well as granites from the literature (Yang et al., 2017) implies that their distinct Mo isotopes are most likely inherited from their magma source (Figs. 7a-b). These trends can be explained by "mixing"

between a depleted end-member with low $^{87}Sr/^{86}Sr$, high $^{143}Nd/^{144}Nd$ and isotopically light Mo and an enriched end-member with high $^{87}Sr/^{86}Sr$, low $^{143}Nd/^{144}Nd$ and isotopically heavy Mo.

It has been suggested that the depleted mantle has a slightly sub-chondritic composition of $\delta^{98/95}Mo$ (-0.21 ± 0.02‰) based on studies of mid-ocean ridge basalts (MORB) and late Archean and Phanerozoic komatiites (Greber et al., 2015; Bezard et al., 2016; McCoy-West et al., 2019; Chen et al., 2022). While the most depleted samples ($\delta^{98/95}Mo$ = -0.26 ± 0.05‰) in the QMS pluton exhibit $\delta^{98/95}Mo$ similar to that of the depleted mantle, they show relatively radiogenic Sr and unradiogenic Nd (εNd(t) <0), differing from the depleted upper mantle. The significant linear trends of $\delta^{98/95}Mo$ with Sr (R^2=0.57) and Nd (R^2=0.79) isotopes defined by the studied samples indicate that the depleted endmember may have lower $\delta^{98/95}Mo$ than depleted upper mantle (Figs. 7a-b). This is further supported by the correlated variations of $\delta^{98/95}Mo$ withRb/La (R^2=0.74) and Ce/Pb (R^2=0.67, negative) for the MME and their host granitoid samples (Figs. 7c-d), which can all be projected to $\delta^{98/95}Mo$ values lower than the depleted mantle (DMM). FreshMORB data (Bezard et al., 2016;) also plot outside the trends defined by the studied samples, suggesting the depleted endmember likely has lower $\delta^{98/95}Mo$ than DMM (Fig. 7).

Freymuth et al. (2015) suggested that the Mo systematics of Mariana arc lavas is mainly controlled by the addition of fluids with heavier Mo derived from the subducting slab and further inferred that the residual ocean crust going through subduction dehydration metamorphism would have low $\delta^{98/95}Mo$ relative to the depleted mantle. Their suggestions have been independently confirmed by a recent study of high-pressure metamorphic rocks from the Raspas complex in Ecuador and the Cabo Ortegal complex in Spain, representing exhumed fragments of subducted ocean crust (Chen et al., 2019). The latter study showed that the eclogites and

blueschists display $\delta^{98/95}$Mo values close to DMM to very low values (~-1‰), which are complementary to the high $\delta^{98/95}$Mo of some arc lavas (Chen et al., 2019). Interestingly, as illustrated in Fig. 7, the ocean crust (OC) residue represented by the eclogites and blueschists (Chen et al., 2019) is characterized by low $\delta^{98/95}$Mo, $^{87}Sr/^{86}Sr$, and Rb/La ratios, high $^{143}Nd/^{144}Nd$ and Ce/Pb ratios, resembling the depleted endmember required for the studied samples. This is consistent with previous suggestions that the most likely melts parental to the MMEs and their host rocks in the two plutons are produced by melting of remaining North Qilian ocean crust together with terrigenous sediments during continental collision (Chen et al., 2015, 2016), which were based on radiogenic isotopes in tandem with petrological and geological evidence. By analogy with the exhumed OC residue in Raspas and Cabo Ortegal (Chen et al., 2019), we can reasonably infer that the remaining North Qilian ocean crust (after subduction-zone dehydration) would have a suitably low $\delta^{98/95}$Mo as the source of the depleted endmember required for the studied samples.

On the other hand, Fig.7 also show that the enriched endmember required for the studied samples from BJS and QMS pluton is characterized by high $\delta^{98/95}$Mo, $^{87}Sr/^{86}Sr$ and Rb/La, and low $^{143}Nd/^{144}Nd$ and Ce/Pb ratios, which is most consistent with the composition of upper continental crust or land derived sediments. It has been suggested that deep-ocean pelagic sediments deposited from oxygenated bottom waters are enriched in isotopically light Mo whereas continental margins generally have sediments with isotopically heavier Mo because of reducing conditions in regions of high primary productivity (upwelling) or basin restriction (see the review from Kendall et al., 2017 and reference therein). For instance, Freymuth et al. (2016) showed that the arc lavas from the Lesser Antilles have remarkably higher $\delta^{98/95}$Mo than the depleted mantle and suggested that they resulted from addition of subducted black shales with

isotopically heavy Mo. While the mass fraction of black shales in the sediment package is less than 10% (Deep Sea Drilling Project Site 144), they are suggested to dominate the Mo budget of the bulk sediment subducting at the Lesser Antilles trench (Freymuth et al., 2016). This suggestion is supported by a subsequent study by Gaschnig et al. (2017), which attributed correlation between Mo isotope and radiogenic isotope of lavas from Lesser Antilles arc to binary mixing between subducting sediment and mantle wedge. Importantly, the high $\delta^{98/95}$Mo values of the Older Arc lavas are suggested to represent greater contribution of subducted Cretaceous black shales (Gaschnig et al., 2017). Accordingly, we hypothesize that the terrigenous sediments that contributed to the studied granitoids have higher $\delta^{98/95}$Mo values (~0.5‰) values (Fig. 7). A detailed Mo isotope survey of these terrigenous sediments in NQOB is necessary but beyond the scope of the present study. To illustrate the arguments above, we attempt to conduct a binary mixing model between the two endmembers for the Mo-Sr isotopic variability. It has been shown that the sedimentary units from DSDP Site 144 display both large compositional and isotopic heterogeneity (Gaschnig et al., 2017), but for simplicity for the modeling, we only considered Mo content variation of the enriched endmember. Our calculations show that 5 % to 15% contribution of Mo from the enriched sediment endmember with 85% to 95% contribution of Mo from the depleted endmember can reproduce the geochemical trends of the data (Fig. 8). It is notable that our samples display strikingly similar trends to I-type granitic rocks from Australia and Scotland reported by Yang et al. (2017) in $\delta^{98/95}$Mo vs. $^{87}Sr/^{86}Sr_{(i)}$ despite their different regional geology (Fig. 8), indicating this two-endmember mixing model may be of general significance for the petrogenesis of I-type granitoids.

5.4 The Mo isotopic composition of continental crust

It has been suggested that shales are ideal materials for estimating average concentrations of fluid-immobile elements of the upper continental crust (e.g., Taylor and McLennan, 1985). Molybdenum, however, is fluid-mobile, and its isotopes can be fractionated during various geological processes such as weathering, riverine transport and deposition (Kendall et al., 2017). The range of $\delta^{98/95}$Mo values in shales is much wider than that observed in igneous rocks (Willbold and Elliott, 2017), making it unfit for constraining the $\delta^{98/95}$Mo value of continental crust. Alternatively, Greber et al. (2014) proposed that the mean molybdenite $\delta^{98/95}$Mo of ca. +0.15‰ can represent a maximum composition of the upper continental crust by arguing that molybdenite forming fluids are fractionated from their source rock. However, recent studies have shown a rather large variation in the $\delta^{98/95}$Mo (>2‰) value of molybdenites (Breillat et al., 2016).

Based on a limited dataset of $\delta^{98/95}$Mo for subduction-related volcanic rocks from their own and published data, and assuming that arc volcanic rocks are a good proxy for the composition of the upper continental crust, Voegelin et al. (2014) proposed a preliminary average value in the $\delta^{98/95}$Mo for the upper continental crust between +0.05 and +0.15‰. However, recent studies have shown a large variability of $\delta^{98/95}$Mo value of arc lavas (Fig. 9), reflecting the complexity of arc lavas with respect to Mo isotopes. This is in keeping with multiple component inputs for arc lavas, i.e., depleted mantle, subducted sediments and slab fluid or melt (Elliott et al., 2003), each of which may have distinct Mo isotopes (Konig et al., 2016). Moreover, it has been argued that the composition of arc lavas cannot represent continental crust as the bulk arc crust is basaltic whereas the bulk continental crust is andesitic (Niu et al., 2013).

Granitoids are the main constituents of the upper continental crust and are suggested to be abundant in the middle and lower crust (Rudnick and Gao, 2004). The average Mo isotopes of granitoids are thus critical for estimating the $\delta^{98/95}$Mo of the igneous upper continental crust. Yang et al. (2017) proposed an estimate of $\delta^{98/95}$Mo = 0.14 ± 0.07‰ (95% c.i., n=55) for the Phanerozoic upper crust based on 52 granites in their study and 6 previously published granites. Incorporation of our new granitoid data into the dataset of previously published granites leaves this estimate largely unchanged ($\delta^{98/95}$Mo =0.12 ± 0.05‰; 95% c.i., n=71). However, it is notable that the available Mo isotopic data in granites displayed large (>1 ‰) Mo isotopic variation even if the three hydrothermally altered samples from Yang et al. (2017) are excluded. This suggests a rather heterogeneous Mo isotopic composition for the continental crust. Thus, more analyses of a wider range of continental crustal samples would be of great significance for refining the estimate of Mo isotopic composition of continental crust.

6 Conclusions

We study the behavior of Mo isotopes during magmatic differentiation, by using well-characterized I-type granitoids and their enclosed MMEs together with analyzing the literature data. The main conclusions are:

(1) The MMEs and their host rocks in each of the two plutons (BJS and QMS) have essentially indistinguishable Mo elemental and isotopic compositions. Combined with re-assessment of published and our newly obtained Mo isotope data, we find no clear evidence of Mo isotope fractionation during fractional crystallization on igneous rocks. We do not wish to conclude from our study that Mo isotopes can never be fractionated during fractional crystallization in all cases, as the current database on this issue is still limited. More studies on

Mo isotopes of well-characterized, cogenetic samples with well-defined liquid lines of descent from varying settings are needed to further address this controversy.

(2) Mo isotopes of the MMEs and their host granitoids from the BJS and QMS plutons correlate positively with Sr isotopes and Rb/La ratios, and negatively with Nd isotopes and Ce/Pb ratios, indicating clearly that compositional variation in the magma source controls the variation of Mo isotope compositions of these granitoids.

(3) Mo isotopes can be used to study magma sources and source histories.

Acknowledgments

We thank Prof. Tim Elliott for providing ^{97}Mo-^{100}Mo double spike and NIST SRM 3134 for Mo isotope analysis. The constructive comments by three anonymous reviewers and the editorial handling by Prof. Catherine Chauvel are gratefully acknowledged. Financial support for this research was provided by the National Natural Science Foundation (NSFC) grants (42176087, 41906050, 41630968, 91958215), China Postdoctoral Science Foundation (2019M652496), NSFC-Shandong Joint Fund for Marine Science Research Centers (U1606401), Youth Innovation Promotion Association, Chinese Academy of Sciences (2021206) and 111 project (B18048).

Declaration of interests

The authors declare that they have no known competing financial interests or personal relationships that could have appeared to influence the work reported in this paper.

References

Alonso-Perez, R., O. Müntener, & P. Ulmer (2009), Igneous garnet and amphibole fractionation in the roots of island arcs: experimental constraints on andesitic liquids, Contributions to

Mineralogy and Petrology, 157(4), 541-558, doi:10.1007/s00410-008-0351-8.
Allègre, C. J. (2008). Isotope geology. Cambridge University Press.
Archer, C., & D. Vance (2008), The isotopic signature of the global riverine molybdenum flux and anoxia in the ancient oceans, Nature Geoscience, 1(9), 597-600, doi:10.1038/ngeo282.
Arnold, G. L., A. Anbar, J. Barling, & T. Lyons (2004), Molybdenum isotope evidence for widespread anoxia in mid-Proterozoic oceans, Science, 304(5667), 87-90.
Barbarin, B. (2005), Mafic magmatic enclaves and mafic rocks associated with some granitoids of the central Sierra Nevada batholith, California: nature, origin, and relations with the hosts, Lithos, 80(1-4), 155-177, doi:10.1016/j.lithos.2004.05.010.
Barbarin, B., & J. Didier (1991), Enclaves of the Mesozoic calc-alkaline granitoids of the Sierra Nevada Batholith, California, Enclaves and granite petrology. Elsevier, Amsterdam, 135, 153.
Barling, J., & A. D. Anbar (2004), Molybdenum isotope fractionation during adsorption by manganese oxides, Earth and Planetary Science Letters, 217(3-4), 315-329, doi:10.1016/s0012-821x(03)00608-3.
Barling, J., G. L. Arnold, & A. Anbar (2001), Natural mass-dependent variations in the isotopic composition of molybdenum, Earth and Planetary Science Letters, 193(3-4), 447-457.
Bezard, R., M. Fischer-Gödde, C. Hamelin, G. A. Brennecka, & T. Kleine (2016), The effects of magmatic processes and crustal recycling on the molybdenum stable isotopic composition of Mid-Ocean Ridge Basalts, Earth and Planetary Science Letters, 453, 171-181, doi:10.1016/j.epsl.2016.07.056.
Breillat, N., C. Guerrot, E. Marcoux, & P. Négrel (2016), A new global database of δ98Mo in molybdenites: A literature review and new data, Journal of Geochemical Exploration, 161, 1-15, doi:10.1016/j.gexplo.2015.07.019.
Burkhardt, C., R. C. Hin, T. Kleine, & B. Bourdon (2014), Evidence for Mo isotope fractionation in the solar nebula and during planetary differentiation, Earth and Planetary Science Letters, 391, 201-211, doi:10.1016/j.epsl.2014.01.037.
Chappell, B., & A. White (1991), Restite enclaves and the restite model, in Enclaves and granite petrology, edited, pp. 479-492, Elsevier Amsterdam.
Chappell, B., & A. White (1992), I-and S-type granites in the Lachlan Fold Belt, Geological Society of America Special Papers, 272, 1-26.
Chappell, B., A. White, & D. Wyborn (1987), The importance of residual source material (restite) in granite petrogenesis, Journal of Petrology, 28(6), 1111-1138.
Chen, B., B. M. Jahn, & K. Suzuki (2013a), Petrological and Nd-Sr-Os isotopic constraints on the origin of high-Mg adakitic rocks from the North China Craton: Tectonic implications, Geology, 41(1), 91-94, doi:10.1130/g33472.1.
Chen, H., P. S. Savage, F.-Z. Teng, R. T. Helz, & F. Moynier (2013b), Zinc isotope fractionation during magmatic differentiation and the isotopic composition of the bulk Earth, Earth and Planetary Science Letters, 369-370, 34-42, doi:10.1016/j.epsl.2013.02.037.
Chen, S., R. C. Hin, T. John, R. Brooker, B. Bryan, Y. Niu, & T. Elliott (2019), Molybdenum systematics of subducted crust record reactive fluid flow from underlying slab serpentine dehydration, Nature Communications, 10(1), 4773, doi:10.1038/s41467-019-12696-3.
Chen, S., Y. Niu, W. Sun, Y. Zhang, J. Li, P. Guo, & P. Sun (2015a), On the origin of mafic magmatic enclaves (MMEs) in syn-collisional granitoids: evidence from the Baojishan pluton in the North Qilian Orogen, China, Mineralogy and Petrology, 109(5), 577-596, doi:10.1007/s00710-015-0383-5.

Chen, S., Y. Niu, & Q. Xue (2018), Syn-collisional felsic magmatism and continental crust growth: A case study from the North Qilian Orogenic Belt at the northern margin of the Tibetan Plateau, Lithos, 308-309, 53-64, doi:10.1016/j.lithos.2018.03.001.

Chen, S., Y. L. Niu, J. Y. Li, W. L. Sun, Y. Zhang, Y. Hu, & F. L. Shao (2016), Syn-collisional adakitic granodiorites formed by fractional crystallization: Insights from their enclosed mafic magmatic enclaves (MMEs) in the Qumushan pluton, North Qilian Orogen at the northern margin of the Tibetan Plateau, Lithos, 248, 455-468, doi:10.1016/j.lithos.2016.01.033.

Chen, S., Niu, Y., Wang, X., Xue, Q. & Sun, W. (2021). Identifying Crystal Accumulation in Granitoids through Amphibole Composition and In Situ Zircon O Isotopes in North Qilian Orogen, Journal of Petrology, 62, 1-18.

Chen, S., Sun, P., Niu, Y., Guo, P., Elliott, T. and Hin, R.C., 2022. Molybdenum isotope systematics of lavas from the East Pacific Rise: Constraints on the source of enriched mid-ocean ridge basalt, Earth and Planetary Science Letters, 578, 117283.

Dahlquist, J. (2002), Mafic microgranular enclaves: early segregation from metaluminous magma (Sierra de Chepes), Pampean Ranges, NW Argentina, Journal of South American Earth Sciences, 15(6), 643-655.

Davidson, J., S. Turner, H. Handley, C. Macpherson, & A. Dosseto (2007), Amphibole "sponge" in arc crust?, Geology, 35(9), 787-790.

Davidson, J., S. Turner, & T. Plank (2013), Dy/Dy*: Variations Arising from Mantle Sources and Petrogenetic Processes, Journal of Petrology, 54(3), 525-537, doi:10.1093/petrology/egs076.

Dodge, F., & R. Kistler (1990), Some additional observations on inclusions in the granitic rocks of the Sierra Nevada, Journal of Geophysical Research: Solid Earth, 95(B11), 17841-17848.

Donaire, T., E. Pascual, C. Pin, & J.-L. Duthou (2005), Microgranular enclaves as evidence of rapid cooling in granitoid rocks: the case of the Los Pedroches granodiorite, Iberian Massif, Spain, Contributions to Mineralogy and Petrology, 149(3), 247-265, doi:10.1007/s00410-005-0652-0.

Elliott, T. (2003). Tracers of the slab. Geophysical Monograph-American Geophysical Union, 138, 23-46.

Fan, J. J., Q. Wang, J. Li, G. J. Wei, D. Wyman, Z. H. Zhao, Y. Liu, J. L. Ma, L. Zhang, & Z. L. Wang (2020), Molybdenum and Boron isotopic compositions of porphyry Cu mineralization - related adakitic rocks in central - eastern China: New insights into their petrogenesis and crust - mantle interaction., Journal of Geophysical Research: Solid Earth, doi:10.1029/2020jb020474.

Freymuth, H., T. Elliott, M. van Soest, & S. Skora (2016), Tracing subducted black shales in the Lesser Antilles arc using molybdenum isotope ratios, Geology, 47(12), 987-990, doi:10.1130/g38344.1.

Freymuth, H., F. Vils, M. Willbold, R. N. Taylor, & T. Elliott (2015), Molybdenum mobility and isotopic fractionation during subduction at the Mariana arc, Earth and Planetary Science Letters, 432, 176-186, doi:10.1016/j.epsl.2015.10.006.

Gaschnig, R. M., Reinhard, C. T., Planavsky, N. J., Wang, X., Asael, D., & Chauvel, C (2017), The molybdenum isotope system as a tracer of slab input in subduction zones: An example from Martinique, Lesser Antilles Arc, Geochemistry, Geophysics, Geosystems, 18(12), 4674-4689.

Goldberg, T., C. Archer, D. Vance, & S. W. Poulton (2009), Mo isotope fractionation during

adsorption to Fe (oxyhydr)oxides, Geochimica et Cosmochimica Acta, 73(21), 6502-6516, doi:10.1016/j.gca.2009.08.004.

Greaney, A. T., R. L. Rudnick, R. M. Gaschnig, J. B. Whalen, B. Luais, & J. D. Clemens (2018), Geochemistry of molybdenum in the continental crust, Geochimica et Cosmochimica Acta, 238, 36-54, doi:10.1016/j.gca.2018.06.039.

Greber, N. D., T. Pettke, & T. F. Nägler (2014), Magmatic–hydrothermal molybdenum isotope fractionation and its relevance to the igneous crustal signature, Lithos, 190-191, 104-110, doi:10.1016/j.lithos.2013.11.006.

Greber, N. D., I. S. Puchtel, T. F. Nägler, & K. Mezger (2015), Komatiites constrain molybdenum isotope composition of the Earth's mantle, Earth and Planetary Science Letters, 421, 129-138, doi:10.1016/j.epsl.2015.03.051.

Grove, T. L., L. T. Elkins-Tanton, S. W. Parman, N. Chatterjee, O. Müntener, & G. A. Gaetani (2003), Fractional crystallization and mantle-melting controls on calc-alkaline differentiation trends, Contributions to Mineralogy and Petrology, 145(5), 515-533.

Hin, R. C., C. Burkhardt, M. W. Schmidt, B. Bourdon, & T. Kleine (2013), Experimental evidence for Mo isotope fractionation between metal and silicate liquids, Earth and Planetary Science Letters, 379, 38-48, doi:10.1016/j.epsl.2013.08.003.

Hou, Q., Y. Chen, Z. Zhao, H. Zhang, & B. Zhang (2006), Indian Ocean-MORB-type isotopic signature of Yushigou ophiolite in North Qilian Mountains and its implications, Sci. China. Ser. D Earth Sci., 49(6), 561-572.

Inglis, E. C., F. Moynier, J. Creech, Z. Deng, J. M. D. Day, F.-Z. Teng, M. Bizzarro, M. Jackson, & P. Savage (2019), Isotopic fractionation of zirconium during magmatic differentiation and the stable isotope composition of the silicate Earth, Geochimica et Cosmochimica Acta, 250, 311-323, doi:10.1016/j.gca.2019.02.010.

König, S., M. Wille, A. Voegelin, & R. Schoenberg (2016), Molybdenum isotope systematics in subduction zones, Earth and Planetary Science Letters, 447, 95-102, doi:10.1016/j.epsl.2016.04.033.

Kendall, B., T. W. Dahl, & A. D. Anbar (2017), The Stable Isotope Geochemistry of Molybdenum, Reviews in Mineralogy and Geochemistry, 82(1), 683-732, doi:10.2138/rmg.2017.82.16.

Lee, C.-T. A., & O. Bachmann (2014), How important is the role of crystal fractionation in making intermediate magmas? Insights from Zr and P systematics, Earth and Planetary Science Letters, 393, 266-274, doi:10.1016/j.epsl.2014.02.044.

Lee, C.-T. A., & D. M. Morton (2015), High silica granites: Terminal porosity and crystal settling in shallow magma chambers, Earth and Planetary Science Letters, 409, 23-31, doi:10.1016/j.epsl.2014.10.040.

Liang, Y.-H., A. N. Halliday, C. Siebert, J. G. Fitton, K. W. Burton, K.-L. Wang, & J. Harvey (2017), Molybdenum isotope fractionation in the mantle, Geochimica et Cosmochimica Acta, 199, 91-111, doi:10.1016/j.gca.2016.11.023.

McCoy-West, A. J., P. Chowdhury, K. W. Burton, P. Sossi, G. M. Nowell, J. G. Fitton, A. C. Kerr, P. A. Cawood, & H. M. Williams (2019), Extensive crustal extraction in Earth's early history inferred from molybdenum isotopes, Nature Geoscience, 12, 946-951, doi:10.1038/s41561-019-0451-2.

Niu, Y., Z. Zhao, D.-C. Zhu, & X. Mo (2013), Continental collision zones are primary sites for net continental crust growth — A testable hypothesis, Earth-Science Reviews, 127, 96-110, doi:10.1016/j.earscirev.2013.09.004.

Pearce, C. R., A. S. Cohen, A. L. Coe, & K. W. Burton (2008), Molybdenum isotope evidence for global ocean anoxia coupled with perturbations to the carbon cycle during the Early Jurassic, Geology, 36(3), 231, doi:10.1130/g24446a.1.

Plank, T., Kelley, K. A., Zimmer, M. M., Hauri, E. H., & Wallace, P. J. (2013), Why do mafic arc magmas contain~ 4 wt% water on average? Earth and Planetary Science Letters, 364, 168-179.

Portnyagin, M., K. Hoernle, S. Storm, N. Mironov, C. van den Bogaard, & R. Botcharnikov (2012), H2O-rich melt inclusions in fayalitic olivine from Hekla volcano: Implications for phase relationships in silicic systems and driving forces of explosive volcanism on Iceland, Earth and Planetary Science Letters, 357-358, 337-346, doi:10.1016/j.epsl.2012.09.047.

Rudnick, R.L., Gao, S., (2004), Composition of the continental crust. In: Rudnick, R.L. (Ed.), Treatise on Geochemistry. Elsevier - Pergamon, Oxford, pp. 1–64.

Savage, P. S., Georg, R. B., Williams, H. M., Burton, K. W., & Halliday, A. N. (2011), Silicon isotope fractionation during magmatic differentiation. Geochimica et Cosmochimica Acta, 75(20), 6124-6139.

Siebert, C., T. F. Nägler, F. von Blanckenburg, & J. D. Kramers (2003), Molybdenum isotope records as a potential new proxy for paleoceanography, Earth and Planetary Science Letters, 211(1-2), 159-171, doi:10.1016/s0012-821x(03)00189-4.

Song, S., Y. Niu, L. Su, & X. Xia (2013), Tectonics of the North Qilian orogen, NW China, Gondwana Research, 23(4), 1378-1401, doi:10.1016/j.gr.2012.02.004.

Taylor, S.R., McLennan, S.M., (1985), The Continental Crust: Its Composition and Evolution. Blackwell, Oxford.

Teng, F.-Z., N. Dauphas, & R. T. Helz (2008), Iron isotope fractionation during magmatic differentiation in Kilauea Iki lava lake, Science, 320(5883), 1620-1622.

Tseng, C.-Y., H.-J. Yang, H.-Y. Yang, D. Liu, C. Wu, C.-K. Cheng, C.-H. Chen, & C.-M. Ker (2009), Continuity of the North Qilian and North Qinling orogenic belts, Central Orogenic System of China: Evidence from newly discovered Paleozoic adakitic rocks, Gondwana Research, 16(2), 285-293, doi:10.1016/j.gr.2009.04.003.

Vernon, R. H. (1983), Restite, xenoliths and microgranitoid enclaves in granites.

Villalobos-Orchard, J., H. Freymuth, B. O'Driscoll, T. Elliott, H. Williams, M. Casalini, & M. Willbold (2020), Molybdenum isotope ratios in Izu arc basalts: The control of subduction zone fluids on compositional variations in arc volcanic systems, Geochimica et Cosmochimica Acta, 288, 68-82, doi:10.1016/j.gca.2020.07.043.

Voegelin, A. R., T. Pettke, N. D. Greber, B. von Niederhäusern, & T. F. Nägler (2014), Magma differentiation fractionates Mo isotope ratios: Evidence from the Kos Plateau Tuff (Aegean Arc), Lithos, 190-191, 440-448, doi:10.1016/j.lithos.2013.12.016.

Wang, Z., J. Ma, J. Li, G. Wei, T. Zeng, L. Li, L. Zhang, W. Deng, L. Xie, & Z. Liu (2018), Fe (hydro) oxide controls Mo isotope fractionation during the weathering of granite, Geochimica et Cosmochimica Acta, 226, 1-17, doi:10.1016/j.gca.2018.01.032.

Willbold, M., & T. Elliott (2017), Molybdenum isotope variations in magmatic rocks, Chemical Geology, 449, 253-268, doi:10.1016/j.chemgeo.2016.12.011.

Willbold, M., K. Hibbert, Y.-J. Lai, H. Freymuth, R. C. Hin, C. Coath, F. Vils, & T. Elliott (2016), High-Precision Mass-Dependent Molybdenum Isotope Variations in Magmatic Rocks Determined by Double-Spike MC-ICP-MS, Geostandards and Geoanalytical Research, 40, 389-403, doi:10.1111/ggr.12109.

Wille, M., O. Nebel, T. Pettke, P. Z. Vroon, S. König, & R. Schoenberg (2018), Molybdenum

isotope variations in calc-alkaline lavas from the Banda arc, Indonesia: Assessing the effect of crystal fractionation in creating isotopically heavy continental crust, Chemical Geology, 485, 1-13.

Xia, L. Q., Z. C. Xia, & X. Y. Xu (2003), Magmagenesis in the Ordovician backarc basins of the Northern Oilian Mountains,China, Geological Society of America Bulletin, 115(12), 1510-1522.

Xia, X., S. Song, & Y. Niu (2012), Tholeiite–Boninite terrane in the North Qilian suture zone: Implications for subduction initiation and back-arc basin development, Chemical Geology, 328(11), 259-277.

Xia, X. H., & S. G. Song (2010), Forming age and tectono-petrogenises of the Jiugequan ophiolite in the North Qilian Mountain, NW China, Science Bulletin, 55(18), 1899-1907.

Xiao, Y., S. Chen, Y. Niu, X. Wang, Q. Xue, G. Wang, Y. Gao, H. Gong, J. Kong, & F. Shao (2020), Mineral compositions of syn-collisional granitoids and their implications for the formation of juvenile continental crust and adakitic magmatism, Journal of Petrology.

Xu, W., S. Gao, Q. Wang, D. Wang, & Y. Liu (2006), Mesozoic crustal thickening of the eastern North China craton: Evidence from eclogite xenoliths and petrologic implications, Geology, 34(9), 721-724.

Yang, J., J. Barling, C. Siebert, J. Fietzke, E. Stephens, & A. N. Halliday (2017), The molybdenum isotopic compositions of I-, S- and A-type granitic suites, Geochimica et Cosmochimica Acta, 205, 168-186, doi:10.1016/j.gca.2017.01.027.

Yang, J., C. Siebert, J. Barling, P. Savage, Y.-H. Liang, & A. N. Halliday (2015), Absence of molybdenum isotope fractionation during magmatic differentiation at Hekla volcano, Iceland, Geochimica et Cosmochimica Acta, 162, 126-136, doi:10.1016/j.gca.2015.04.011.

Yin, A., & T. M. Harrison (2000), Geologic Evolution of the Himalayan-Tibetan Orogen, Annual Review of Earth & Planetary Sciences, 28(28), 211-280.

Yu, S., J. Zhang, H. Qin, D. Sun, X. Zhao, F. Cong, & Y. Li (2015), Petrogenesis of the early Paleozoic low-Mg and high-Mg adakitic rocks in the North Qilian orogenic belt, NW China: Implications for transition from crustal thickening to extension thinning, Journal of Asian Earth Sciences, 107, 122-139, doi:10.1016/j.jseaes.2015.04.018.

Zhang, Y., C. Yuan, M. Sun, J. Li, X. Long, Y. Jiang, & Z. Huang (2020), Molybdenum and boron isotopic evidence for carbon-recycling via carbonate dissolution in subduction zones, Geochimica et Cosmochimica Acta, doi:10.1016/j.gca.2019.12.013.

Figure captions

Fig. 1. (a) Simplified geological map of the North Qilian Orogen showing distribution of the main tectonic units (modified after Song et al., 2013; Chen et al., 2016). (b) Simplified map of the Qumushan (QMS) and Baojishan (BJS) areas in the eastern section of the North Qilian Orogen showing sample locations for BJS pluton and QMS pluton (Table A1).

Fig. 2. Plots of (a) Mo vs. SiO_2, (b) Dy/Dy* vs. SiO_2, (c) Mo vs. Dy/Dy* and (d) Mo vs. K/Rb. Major and trace elements for BJS and QMS pluton are from Chen et al. (2015, 2016) and compiled in Table A1. The grey circles in (a) and (d) are literature data on the granitoids (Yang et al., 2017).

Fig. 3. Plots of (a) $\delta^{98/95}$Mo vs. SiO_2, (b) $\delta^{98/95}$Mo vs. K/Rb, (c) $\delta^{98/95}$Mo vs. Dy/Dy* and (d) $\delta^{98/95}$Mo vs. $Fe_2O_3^T$. Literature data for granitoids are the same as in Fig. 2.

Fig. 4. Plots of Mo (a), $\delta^{98/95}$Mo (b), Dy/ Yb (c) and Dy/Dy* (d) vs. SiO_2 for lavas from different

arcs (Kos, Mariana, Banda, Izu and the Lesser Antilles), Hekla (Iceland) and MORB. Data sources: Kos (Voegelin et al., 2014); Mariana (Freymuth et al., 2015); Banda (Wille et al., 2018); Izu (Villalobos-Orchard et al., 2020); Lesser Antilles (green squares: Freymuth et al., 2016; yellow squares: Gaschnig et al., 2017); Hekla (Yang et al., 2015); MORB (Bezard et al., 2016).

Fig. 5. Plots of (a) $\delta^{98/95}$Mo vs. Dy/Dy*, (b) $\delta^{98/95}$Mo vs. Dy/Yb, (c) $\delta^{98/95}$Mo vs. Mo/Ce for lavas from different arcs (Kos, Mariana, Banda, Izu and the Lesser Antilles), Hekla (Iceland) and MORB. Data sources are the same as in Fig. 4.

Fig. 6. Plots of $\delta^{98/95}$Mo vs. Dy/Dy*, Dy/ Yb for lavas from Kos (Voegelin et al., 2014) and Hekla (Yang et al., 2015) . Several model crystallization trajectories are illustrated using equations (1-3) with different parameters. The partition coefficients for amphibole (D^{La}_{Amp} =0.245, D^{Dy}_{Amp} =2.225, D^{Yb}_{Amp} =1.625) and biotite (D^{La}_{Bt} =0.318, D^{Dy}_{Bt} =0.097, D^{La}_{Bt} =0.670) are from Chen et al. (2016) and reference therein. The fractionation factors for Mo isotopes for amphibole ($\alpha_{amphibole\text{-}melt}$ = 0.9995) and biotite ($\alpha_{biotite\text{-}melt}$ = 0.9997) are from Voegelin et al. (2014). The partition coefficient of Mo for amphibole in (a-b) ranges from 0.1 to 0.3 (number along lines). For simplicity, the best estimated D^{Mo} for amphibole (D^{Mo}_{Amp} =0.1) and biotite (D^{Mo}_{Bt} =0.15) determined by Vogelin et al. (2014) is used in (c-d). Marks on the fractional crystallization trends represent increments of 10% fractionation. F is the fraction of melt remaining. The samples with the lowest SiO_2 contents from Kos island and Hekla are used as the initial composition of their parental melt, respectively. Error bars represent the external reproducibility.

Fig. 7. Plots of (a) $\delta^{98/95}$Mo vs. $^{87}Sr/^{86}Sr_{(i)}$, (b) $\delta^{98/95}$Mo vs. $\varepsilon Nd_{(t)}$, (c) $\delta^{98/95}$Mo vs. Rb/La, (d) $\delta^{98/95}$Mo vs. Ce/Pb. Values for granitoids, Depleted MORB mantle (DMM), Mid-ocean Ridge Basalts (MORB) and Oceanic crust (OC) residues are also plotted for reference. Dash lines are linear (a-b) and logarithmic (c-d) regressions through the granitoids and MME from the two plutons. All Sr and Nd isotopes of our samples are corrected to 430 Ma, corresponding to the U-Pb zircon age of samples from PCS and QMS plutons (Chen et al., 2015, 2016). Data sources: Granitoids (Yang et al., 2017), MORB (Bezard et al. 2016), DMM (Willbold and Elliott, 2017; Workman 2005). OC residues (Chen et al., 2019 and references therein). Error bars represent the external reproducibility.

Fig. 8. Plot of $\delta^{98/95}$Mo vs. $^{87}Sr/^{86}Sr(i)$ showing models for binary mixing of a depleted end-member (OC residue) with hypothetical sediment. The hypothetical depleted endmember is represented by the average composition of ocean crust residue (eclogite and blueschist) from Chen et al. (2019) with Sr=12.6 ppm, Mo=0.14 ppm and $^{87}Sr/^{86}Sr_{(i)}$=0.7043. The hypothetical sediment endmember is represented by the average composition of global subducting sediment (GLOSS) (Plank and Langmuir, 1998) with Sr=327 ppm and $^{87}Sr/^{86}Sr_{(i)}$=0.7173. The hypothesized sediment endmember is assumed to have high $\delta^{98/95}$Mo (0.50‰), based on a linear mixing array. Given Mo concentration of sediment show a large variation of Mo concentration, varying Mo contents of sediment are used for modeling. $f = [Mo]_{sediment}/[Mo]_{depleted\ endmember}$. The ticks on modeling curves represent 5% increments of the depleted end-member during mixing.

Fig. 9. Histogram of $\delta^{98/95}$Mo values of granitoids (a) and subduction-related arc lavas (b). Data sources: granitoids are from this study and Yang et al. (2017), excluding three hydrothermally altered samples; arc lavas are from Voegelin et al. (2014), Freymuth et al. (2015, 2016), König et al. (2016), Gaschnig et al. (2017), Wille et al. (2018) and Villalobos-Orchard et al. (2020).

Supplementary materials

Fig. A1. Photomicrographs showing petrographic characteristics of the MMEs and their host granitoids from the BJS and QMS plutons (left panels), and pie charts of mineral abundance (by volume) determined by TIMA (Chen et al., 2021) for the whole thin section (right panels). The first two rows and the last two rows are the host granitoids and their enclosed MMEs from BJS and QMS plutons, respectively. Amp=amphibole; Bt=biotite; Pl=plagioclase; Qz=quartz.

Fig. A2. Classification diagrams of the host granitoids and the MMEs in the QMS and BJS pluton. (a) Total alkalis vs. SiO_2 (Le Maitre et al., 1989), (b) K_2O vs. SiO_2, and (c) A/NK vs. A/CNK. Data sources are listed in Table A1.

Fig. A3. Plots of (a) bull-rock $^{87}Sr/^{86}Sr_{(i)}$ vs. SiO_2, (b) bull-rock $\varepsilon Nd_{(t)}$ vs. SiO_2, and (c) zircon in-situ O isotopes of the MMEs and their host granitoids in the QMS and BJS pluton. Data sources are listed in Table A1.

Fig. A4. Plots of (a) $\delta^{98/95}Mo$ vs. LOI and (b) $\delta^{98/95}Mo$ vs. CIA of the host granitoids and the MMEs in the QMS and BJS pluton. Data sources are listed in Table A1.

Table captions

Table A1. Summary of bulk-rock geochemical data, zircon U-Pb ages and zircon O isotopes for granitoids and their enclosed MME from BJS and QMS in this study**.**

Table A2. Molybdenum isotope and concentration data for granitoids and their enclosed MME from BJS and QMS in this study.

Declaration of interests

☒ The authors declare that they have no known competing financial interests or personal relationships that could have appeared to influence the work reported in this paper.

☐The authors declare the following financial interests/personal relationships which may be considered as potential competing interests:

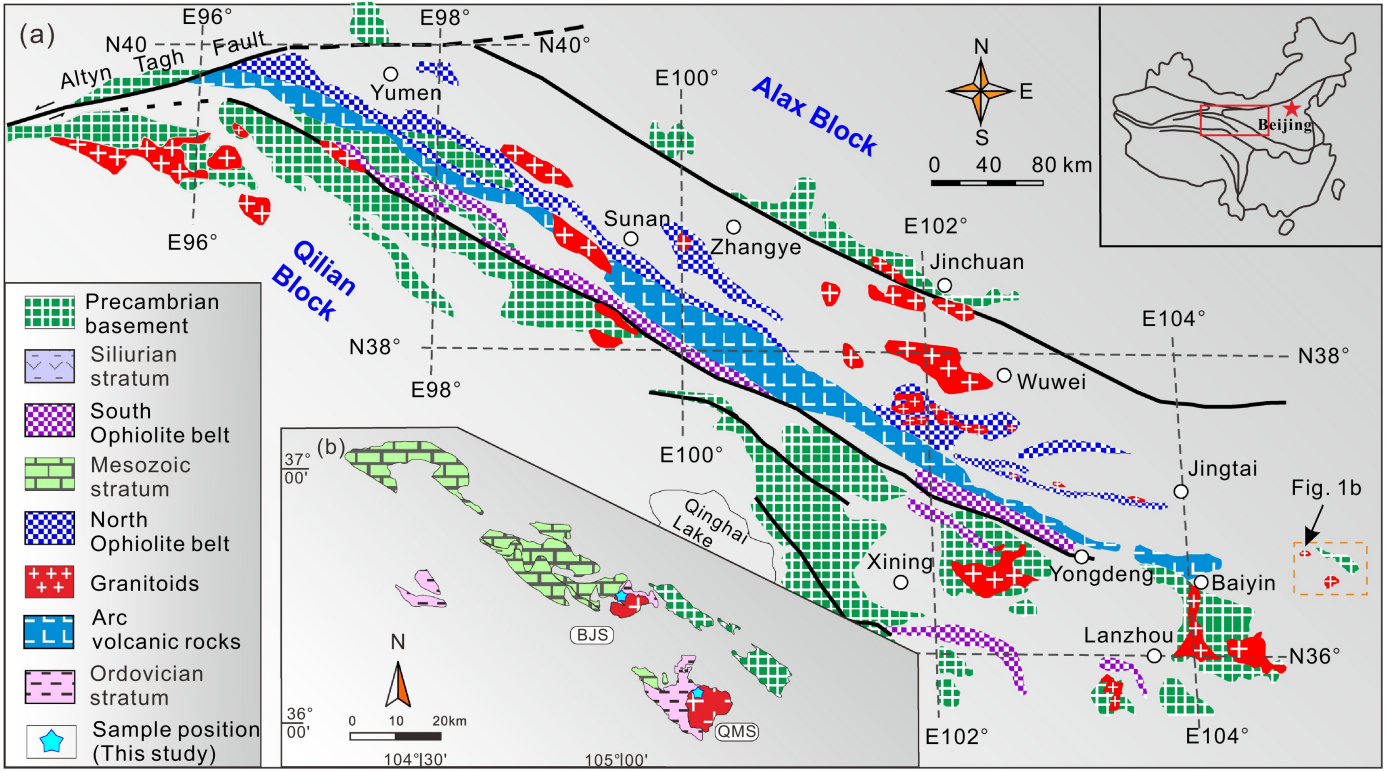
(a)
Altyn Tagh Fault
N40
E96°
E98°
E100°
E102°
E104°
N38°
N36°
Yumen
Sunan
Zhangye
Jinchuan
Wuwei
Jingtai
Xining
Yongdeng
Baiyin
Lanzhou
Alax Block
Qilian Block
N
E
S
0 40 80 km
Beijing
Fig. 1b
Precambrian basement
Siliurian stratum
South Ophiolite belt
Mesozoic stratum
North Ophiolite belt
Granitoids
Arc volcanic rocks
Ordovician stratum
Sample position (This study)
(b)
37° 00'
36° 00'
Qinghai Lake
BJS
QMS
N
0 10 20km
104°30'
105°00'

Figure 1

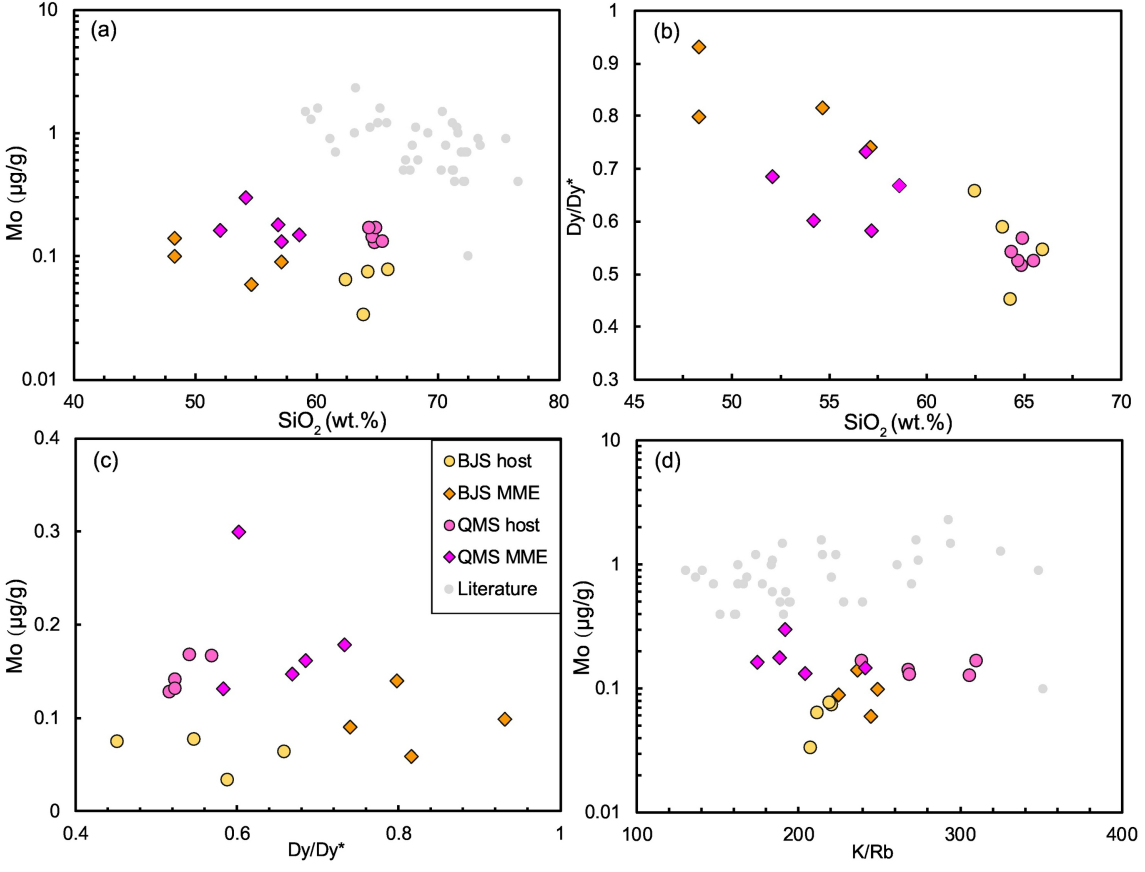
(a)
Mo (μg/g)
SiO2 (wt.%)
(b)
Dy/Dy*
SiO2 (wt.%)
(c)
Mo (μg/g)
Dy/Dy*
BJS host
BJS MME
QMS host
QMS MME
Literature
(d)
Mo (μg/g)
K/Rb

Figure 2

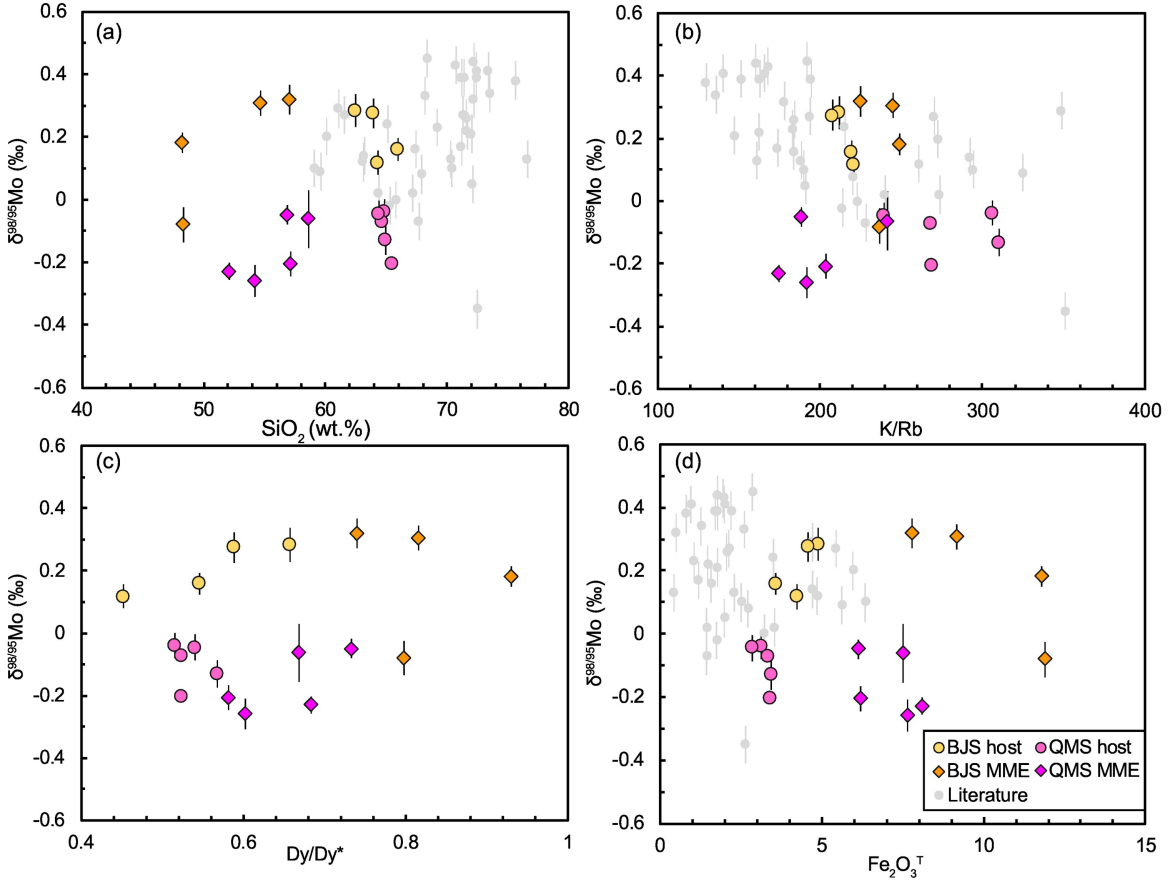
(a)
(b)
(c)
(d)
δ98/95Mo (‰)
SiO2 (wt.%)
K/Rb
Dy/Dy*
Fe2O3T
BJS host
QMS host
BJS MME
QMS MME
Literature

Figure 3

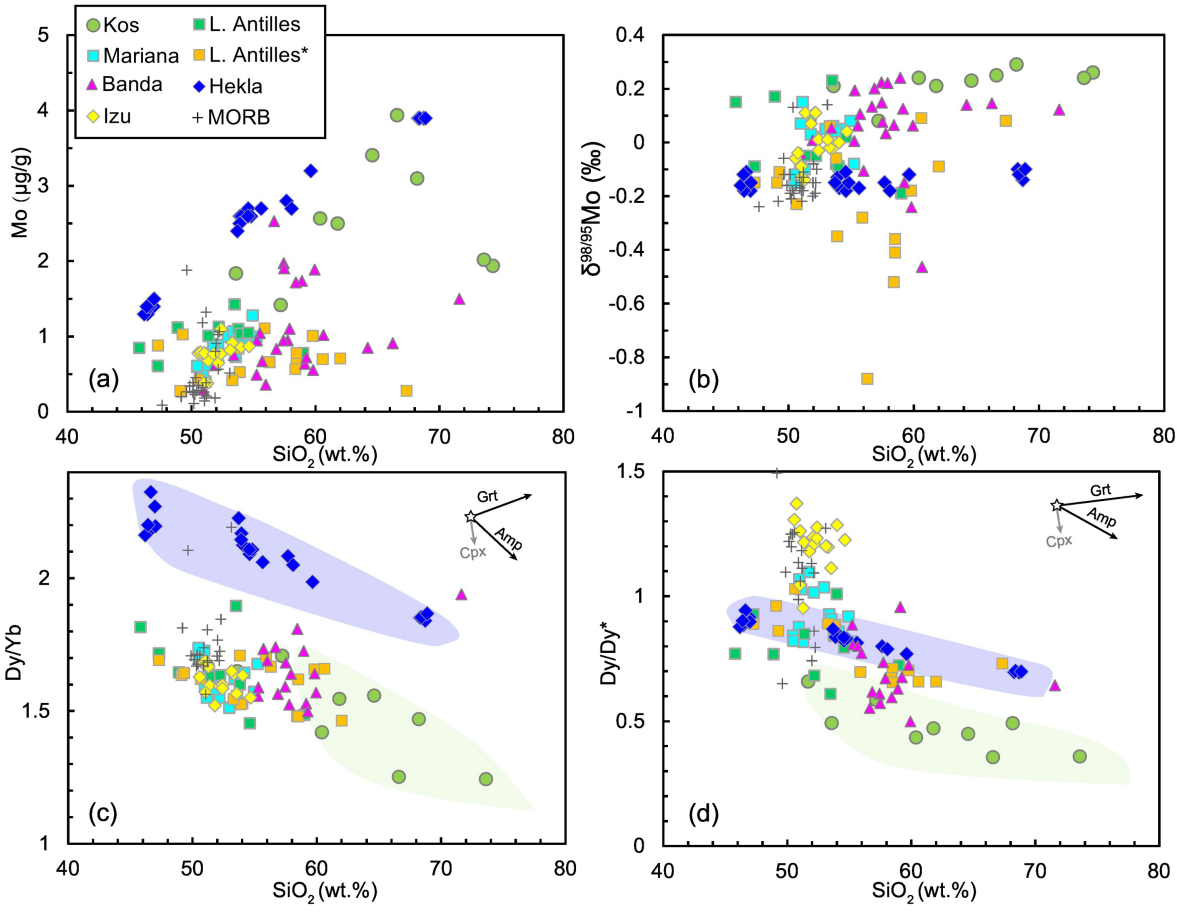
Kos
L. Antilles
Mariana
L. Antilles*
Banda
Hekla
Izu
MORB
Mo (µg/g)
(a)
SiO2 (wt.%)
δ98/95Mo (‰)
(b)
Dy/Yb
(c)
Grt
Amp
Cpx
Dy/Dy*
(d)

Figure 4

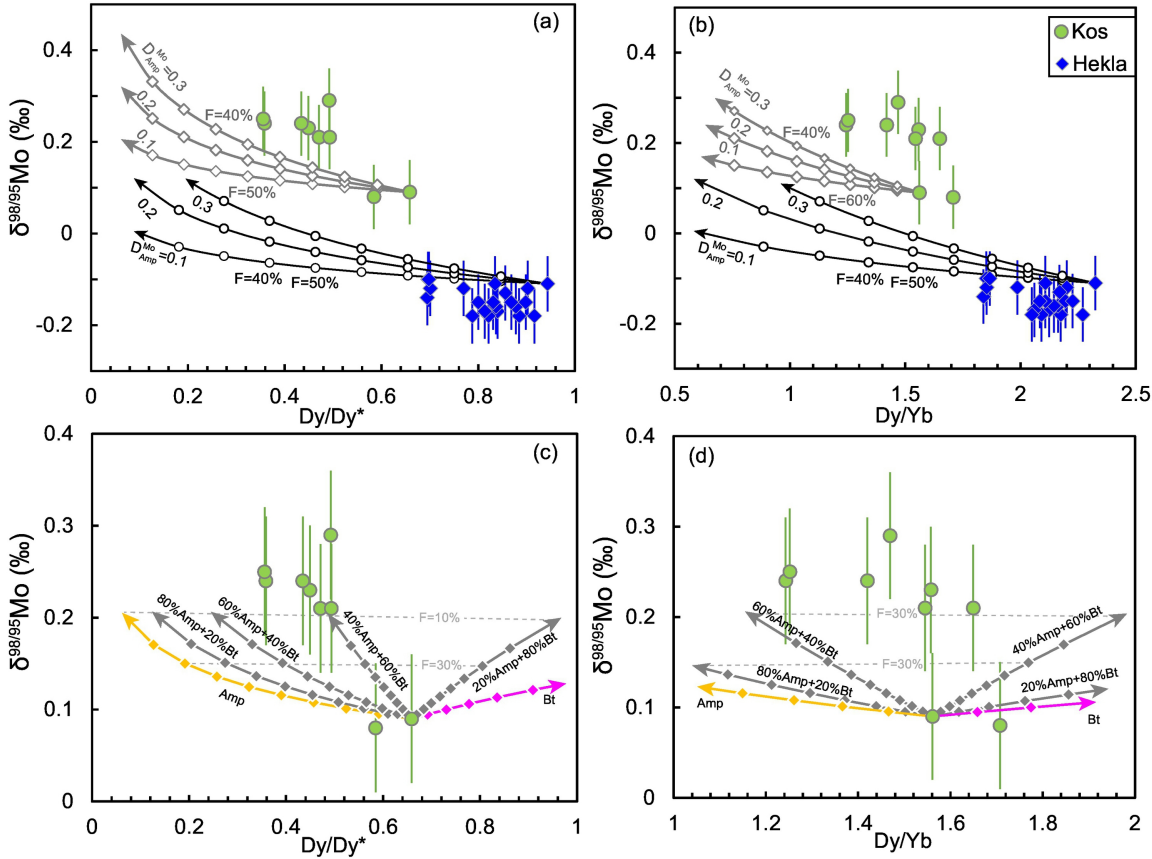
(a)
(b)
(c)
(d)
Kos
Hekla
δ98/95Mo (‰)
Dy/Dy*
Dy/Yb
F=40%
F=50%
F=60%
F=10%
F=30%
Amp
Bt
80%Amp+20%Bt
60%Amp+40%Bt
40%Amp+60%Bt
20%Amp+80%Bt

Figure 5

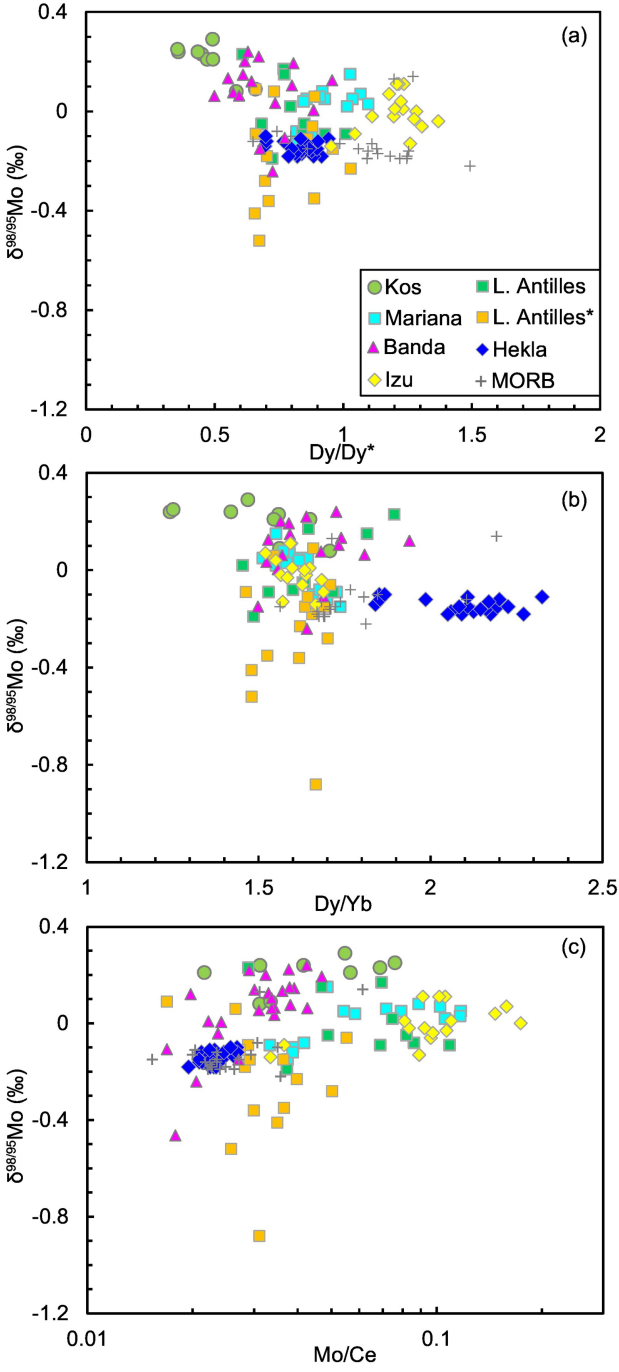
(a)
δ98/95Mo (‰)
Dy/Dy*
Kos
L. Antilles
Mariana
L. Antilles*
Banda
Hekla
Izu
MORB
(b)
δ98/95Mo (‰)
Dy/Yb
(c)
δ98/95Mo (‰)
Mo/Ce

Figure 6

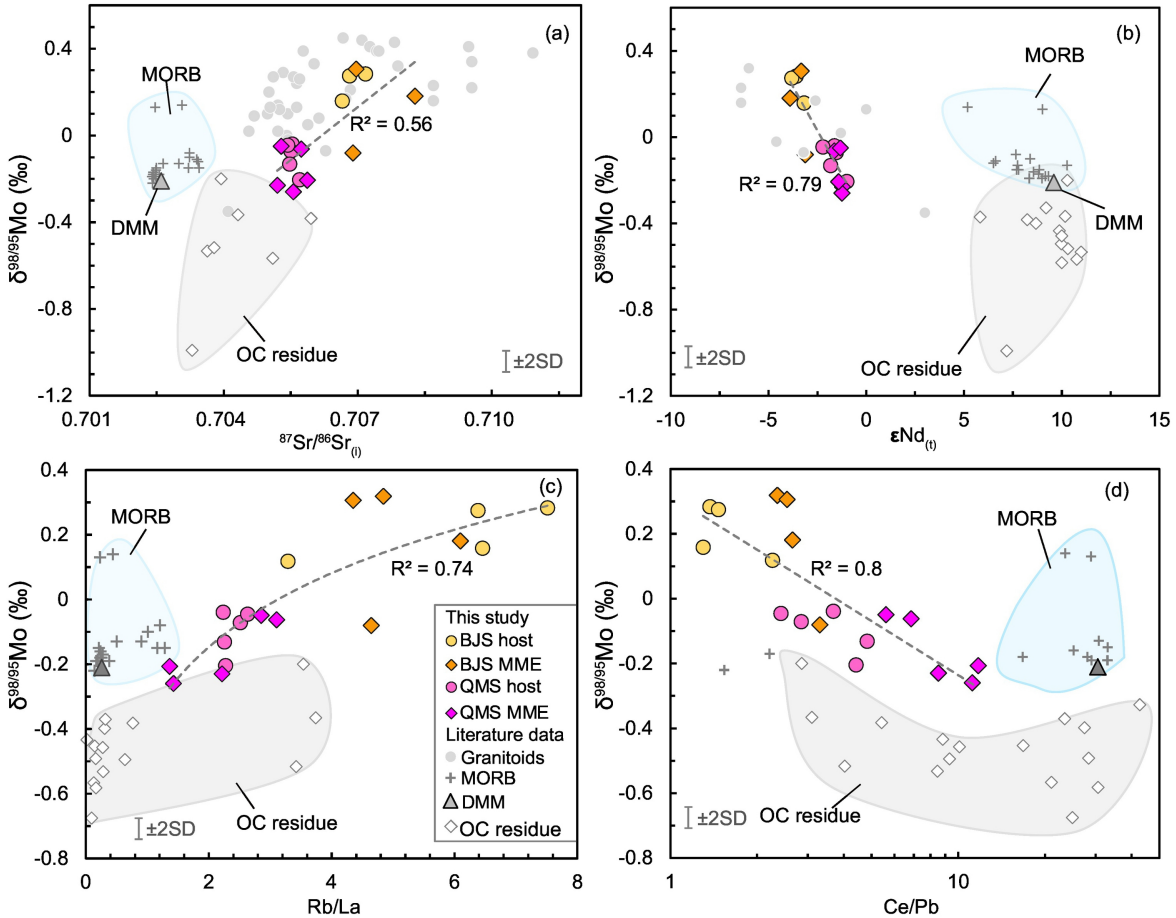
(a)
MORB
DMM
R² = 0.56
OC residue
±2SD
δ98/95Mo (‰)
87Sr/86Sr(i)
(b)
MORB
DMM
R² = 0.79
OC residue
±2SD
εNd(t)
(c)
MORB
R² = 0.74
OC residue
±2SD
This study
BJS host
BJS MME
QMS host
QMS MME
Literature data
Granitoids
MORB
DMM
OC residue
Rb/La
(d)
MORB
R² = 0.8
OC residue
±2SD
Ce/Pb

Figure 7

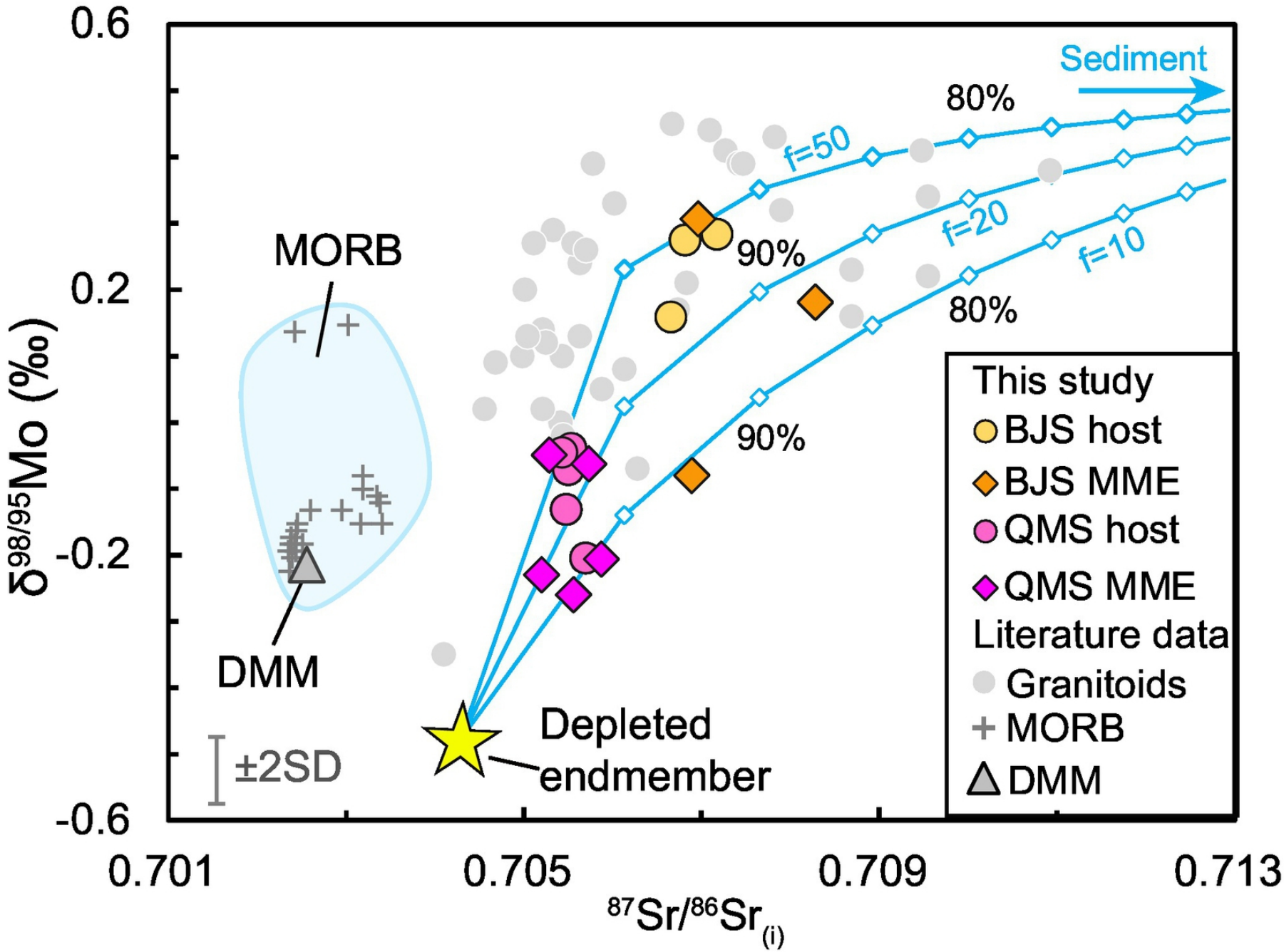
0.6
0.2
-0.2
-0.6
0.701
0.705
0.709
0.713
$\delta^{98/95}$Mo (‰)
$^{87}Sr/^{86}Sr_{(i)}$
Sediment
80%
f=50
90%
f=20
f=10
80%
90%
MORB
DMM
±2SD
Depleted
endmember
This study
BJS host
BJS MME
QMS host
QMS MME
Literature data
Granitoids
MORB
DMM

Figure 8

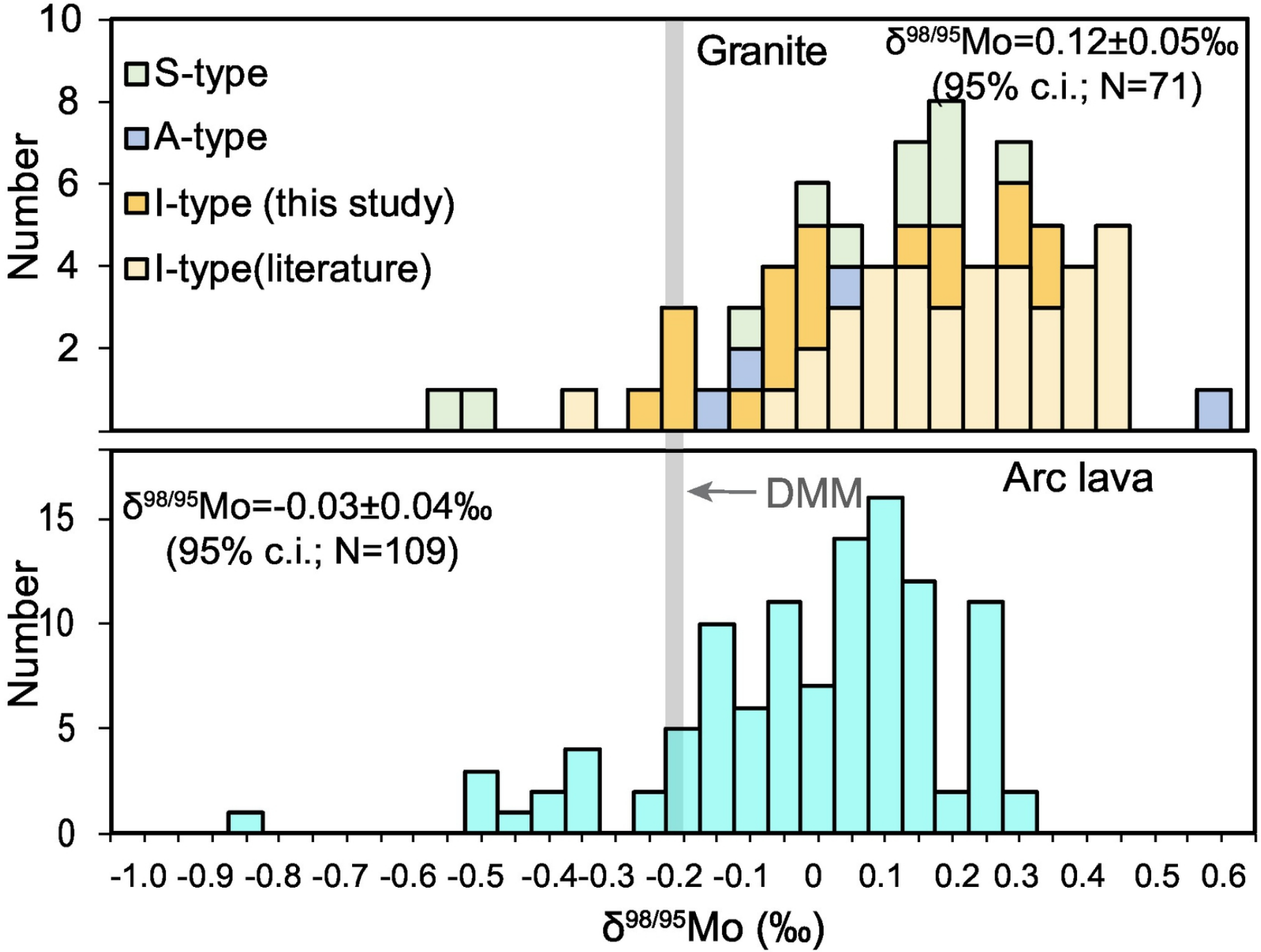
Granite
δ98/95Mo=0.12±0.05‰
(95% c.i.; N=71)
S-type
A-type
I-type (this study)
I-type(literature)
Number
Arc lava
δ98/95Mo=-0.03±0.04‰
(95% c.i.; N=109)
DMM
δ98/95Mo (‰)

Figure 9